Tracer diffusion of oxygen in CoO-SiO_2 melts

1994 J. Phys.: Condens. Matter 6 9825

(http://iopscience.iop.org/0953-8984/6/46/003)

J. Phys.: Condens. Matter 6 (1994) 9825–9834. Printed in the UK

Tracer diffusion of oxygen in $CoO–SiO_2$ melts

T F Young†‡, J Kieffer†§ and G Borchardt†

† Institut für Allgemeine Metallurgie, Technische Universität Clausthal, D-38678 Clausthal–Zellerfeld, Germany

‡ Department of Physics, National Sun Yat-Sen University, Kaohsiung, Taiwan, Republic of China 80424

§ Department of Materials Science and Engineering, University of Illinois, Urbana, IL 61801, USA

Received 17 March 1994, in final form 5 July 1994

Abstract. Tracer diffusion of oxygen in $CoO–SiO_2$ silicate melts has been studied in the composition range of $0.3 \leqslant X_{SiO_2} \leqslant 0.45$ (X = mole fraction) at 1450 to 1550 °C. Experiments were carried out using a capillary–reservoir method, involving a specially designed capillary to avoid convection effects. ^{18}O diffusion profiles were obtained from secondary-ion mass spectrometric analysis. Effective diffusivities, $D^*_{O,eff}$, were obtained by fitting these profiles to the appropriate solutions of Fick's second law. The effective diffusivity of oxygen was found to be smaller than that of cobalt, but larger than that of silicon. The composition dependence of the activation energies for oxygen diffusion, E_A, is significantly different from those of silicon or cobalt: the variation of E_A with the composition was less in the case of oxygen. Experimentally determined diffusion profiles have been compared to those of computer simulations that are based on a kinetic model. The agreement between the shapes of the experimental and simulated concentration profiles, as well as the similarity in the composition dependence of experimental and simulated $D^*_{O,eff}$, is evidence for the strong tendency towards polycondensation in cobalt silicate melts.

1. Introduction

The physical and chemical properties of silicate melts are of considerable significance for a great variety of technological applications, and they are very important for the understanding of geophysical and petrological phenomena. Properties such as viscosity, diffusivity, electrical and thermal conductivity are strongly affected by the chemical composition, pressure and temperature. A number of models for the structures of silicate melts have been developed based on experimental data of thermodynamic properties [1–6].

The nature of silicate melts may be better understood by examining the relationships between their structures and the mobilities of the structural constituents, which can be measured during self- and interdiffusion processes. The basic structure of silicate melts is the SiO_4^{4-} tetrahedron. This anion unit is able to share its oxygen atoms with other silicon atoms in a polymerized chain, forming complex polyanions of various sizes. From this, it may be inferred that the transport properties of quasibinary silicate melts $MO–SiO_2$ depend on the nature of the cation (M) and, for a given cation, on the ratio of MO to SiO_2, as well as on the temperature.

In literature relating to the transport properties of quasibinary silicate melts, there is only one system, $PbO–SiO_2$ at 850 °C, that has been thoroughly studied by the group of Schmalzried [7–9]. In addition to this study, other significant investigations include the

0953-8984/94/469825+10$19.50

tracer diffusion and electrical conductivity measurements in the system $CaO–SiO_2$ at 1600 °C by Schwerdtfeger and Keller [10–12], and the chemical diffusion and tracer diffusion of binary alkali silicate melts $MO–SiO_2$ by Frischat's group [13].

Recently, Kieffer and Borchardt investigated diffusion in $CoO–SiO_2$ melts [14, 15]. $CoO–SiO_2$ is a model system for process metallurgy and glass production, because cobalt, like iron, exists in silicate melts in more than one oxidation state. Kieffer and Borchardt measured tracer diffusivities of Si and Co at different temperatures and at different compositions. In order to interpret their experimental findings, they formulated a kinetic model [16] for binary silicate melts, which relates the details of the silicon mass transport to the polyanionic melt structure. The equilibrium distribution of polyanions can also be derived from this model, and this distribution agrees qualitatively with that obtained from thermodynamic calculations [1–6].

In this paper we report on our experimental investigation of the ^{18}O tracer diffusion in $CoO–SiO_2$ melts as a function of temperature and composition. The kinetic model mentioned above has been extended by the present authors to describe tracer diffusion of both oxygen and silicon in binary silicate melts by means of computer simulation (see the following paper [17]). The results of these computer simulations are compared with experimental data, providing explanations for the structural and compositional dependence of elemental mobilities.

2. Experimental details

In this work two major difficulties associated with $CoO–SiO_2$ melts had to be dealt with: first, prevention of spurious results associated with convection during the diffusion experiment; and secondly, avoidance of the detrimental effects of gas bubbles that form and rise in the melts during cooling and upon solidification. The physical solubility of oxygen in the liquid silicate is greater than that in the solid. Owing to the reaction

$$4Co^{3+} + 2O^{2-} \rightarrow 4Co^{2+} + O_2(g)$$

chemically formed oxygen is released if the temperature is lowered below the liquidity of phases that involve divalent cobalt. In order to make a microscopic analysis (secondary-ion mass spectrometry, SIMS), however, a fine grain structure of the sample through a rapid quench is desirable. In earlier investigations, Kieffer successfully solved this problem by using a specially designed capillary [14]. His design allows the excess gas to escape through lateral slits, perpendicular to the diffusion path (see figure 1(*a*)).

In comparison to the Si and Co tracer diffusion experiments, the set-up for the oxygen tracer diffusion experiment is more complicated, owing to the precautions required for the preparation and maintenance of tracer sources. The argon atmosphere used in the experiment contained oxygen (partial pressure of oxygen is about 1 Pa), and hence exchange reactions between this atmospheric oxygen and the tracer oxygen in the melt are likely to occur wherever the melt is exposed to the furnace atmosphere. Therefore, the earlier capillary design, developed by Kieffer, was not suitable for the present oxygen diffusion experiment, as it has an 'open' edge. To solve this problem, while preventing bubble formation and the associated convection during the quench of the sample, a new type of capillary was developed. It consisted of a central cylindrical part and two radial wedge-shaped fins (see figure 1(*b*)). Upon rapid cooling, the melt in the fins immediately solidified and the gas was released towards the central part of the capillary. Bubbles that formed here could either rise through the central part, as long as the melt remained liquid, or eventually got trapped upon solidification. With this procedure, the outermost parts of the fins were free of gas bubbles and the isotope profiles could be analysed without difficulty.

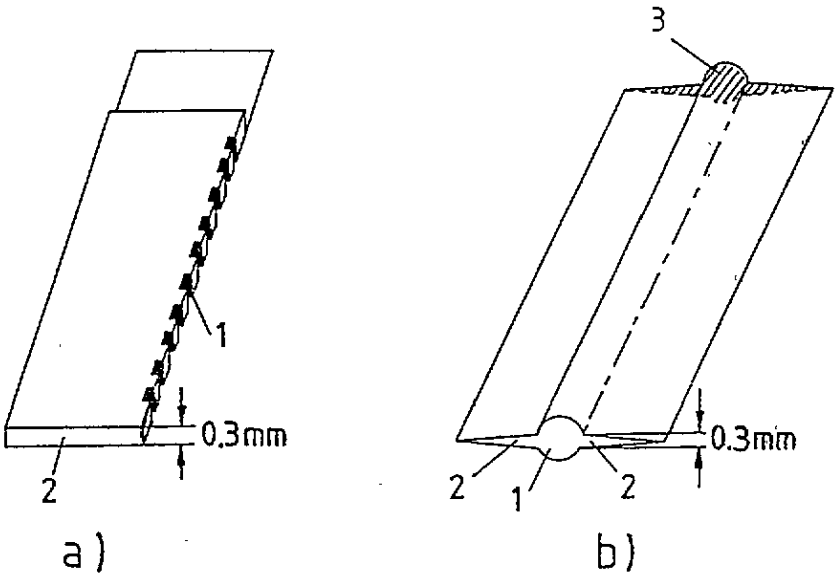

Figure 1. Schematic diagrams of the forms of Pt–Rh capillaries. (*a*) For Co and Si diffusion experiment by Kieffer [14]. (*b*) For O diffusion in this work: 1, cylindrical part, open side; 2, fins; 3, closed side.

2.1. Oxygen diffusion experiments

To minimize costs, and to maintain a reasonable accuracy, a capillary–reservoir method was chosen, where the ^{18}O-bearing melt was placed in the capillary. The ^{18}O isotope was introduced in two different ways. The first way was the oxidation of Co powder according to the reaction:

$$2Co + O_2^*(g) \rightarrow 2CoO^* \tag{1}$$

In second approach the ^{18}O was combined with silicon according to the reaction:

$$SiCl_4 + 2H_2O^* \rightarrow SiO_2^* + 4HCl(g) \tag{2}$$

In both cases we used a 50:50 mixture of $^{18}O_2$ and $^{16}O_2$ (Ventron GmbH, Karlsruhe, Germany).

The oxide mixture used for the reservoir melts was prepared via a gel method, using spectrally pure materials. An alloy of Pt–20% Rh was used as the material for the reservoir crucible and for the capillary. The capillary was cut from a Pt–20% Rh tube (diameter 4.5 mm, thickness 0.1 mm). After cleaning, it was shaped according to the diagram in figure 1(*b*), and one end was closed by welding.

Known amounts of cobalt and silica powder were mixed, ground, die pressed into pellets, and placed into a vertical vacuum tube furnace. In the furnace the pellets were heated in a gas atmosphere of $^{18}O_2/^{16}O_2$ and 99.999% argon at 1200 °C. A quadrupole mass spectrometer was used to monitor the oxidation reaction and a closed-cycle pumping system was designed, allowing one to collect and re-use the gas mixture. After oxidation, the pellets were ground and filled into the capillary. The capillary was then placed into the furnace for melting. Subsequently, the capillary was lowered into the cooler zone of the

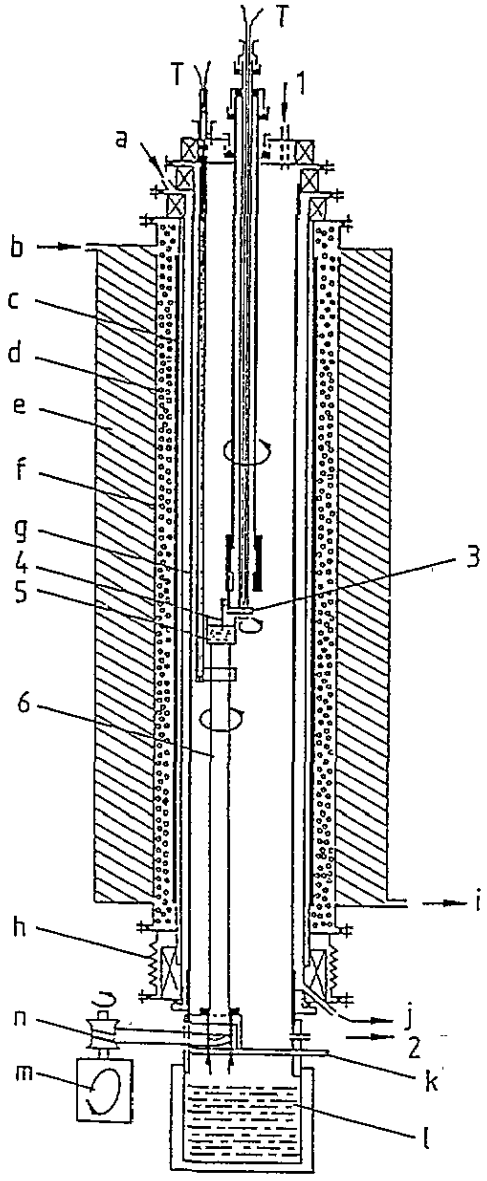

1	working atmosphere, gas inlet: Ar + O_2 (P_{O_2}= 1 Pa)
2	gas outlet: Ar + O_2 (s. 1)
3	rotating sample holder
4	sample capillary
5	melt reservoir
6	Al_2O_3 holder of crucible
a	Ar buffer gas of working tube, gas inlet
b	protective gas (Ar + 5% H_2) for Mo heating element, gas inlet
c	Mo heating element
d	Al_2O_3 insulation
e	Al_2O_3 - SiO_2 insulation
f	steel tube
g	reaction tube (Al_2O_3)
h	compensator
i	protective gas (outlet)
j	Ar buffer gas (see a), gas outlet
k	shutter
l	quench oil
m	motor
n	transmission
T	thermocouple

Figure 2. Furnace for diffusion experiments after the capillary–reservoir method.

furnace to solidify with the solidification front slowly moving upwards. This process was necessary to get a bubble-free silicate in the capillary.

Figure 2 shows the details of the experimental apparatus. A slot was machined into the bottom part of the sample holder (3), which allowed one to release the capillary for a rapid quench (see figure 3). An electric probe (34) was used to act as a contact sensor for positioning the sample relative to the reservoir. The partial pressure of the oxygen used was adjusted to about 1 Pa. The sample was preheated at 1350 °C for 10 min, and was then moved to the hot zone of the furnace. Within 1 min, its temperature was raised to 1450 °C. After attaining this temperature, the sample was immersed into the reservoir melt.

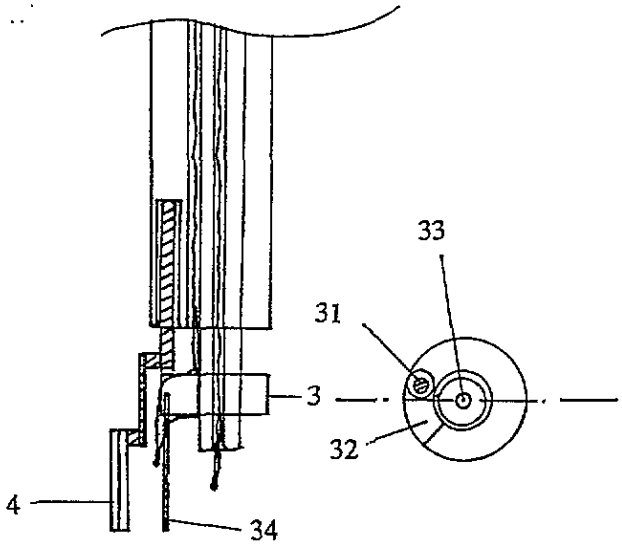

Figure 3. Schematic diagram of sample holder (3): 31 and 4, sample capillary; 32, slot of supporter; 33, thermocouple; 34, electric contact probe (see text).

At this moment the actual diffusion experiment began. In order to maintain a well defined experimental boundary condition of constant ^{18}O concentration, the reservoir crucible was rotated during the experiment at two cycles per minute, by means of a motor connected to the supporting pedestal. At the end of the diffusion experiment, the sample was taken out of the reservoir melt (5), and the holder (3) was moved away by rotation, in such a way that the sample was dropped through the slot (32) and fell into a quenching oil well (see 1 in figure 2).

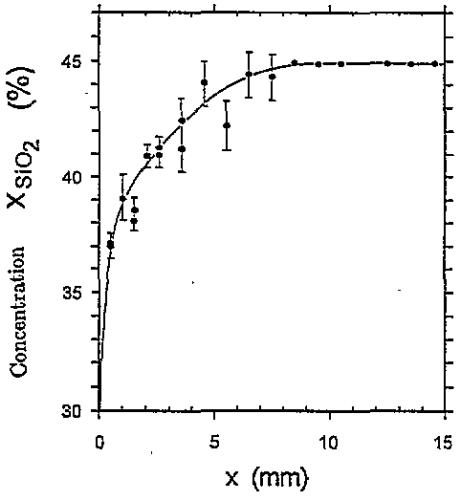

Figure 4. Concentration profile resulting from chemical diffusion.

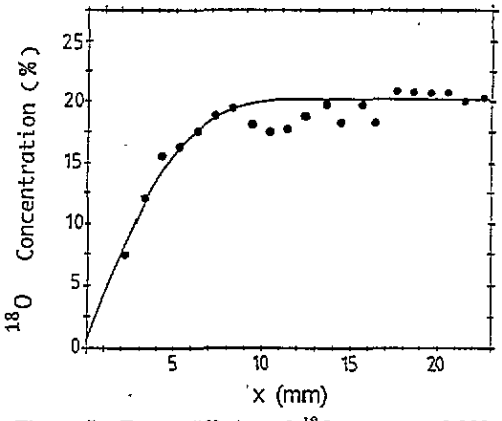

Figure 5. Tracer diffusion of ^{18}O: $X_{SiO_2} = 0.333$, $T = 1503\,°C$, $t = 3620$ s, $D_{^{18}O} = (2.33 \pm 0.52) \times 10^{-5}$ cm^2 s^{-1}.

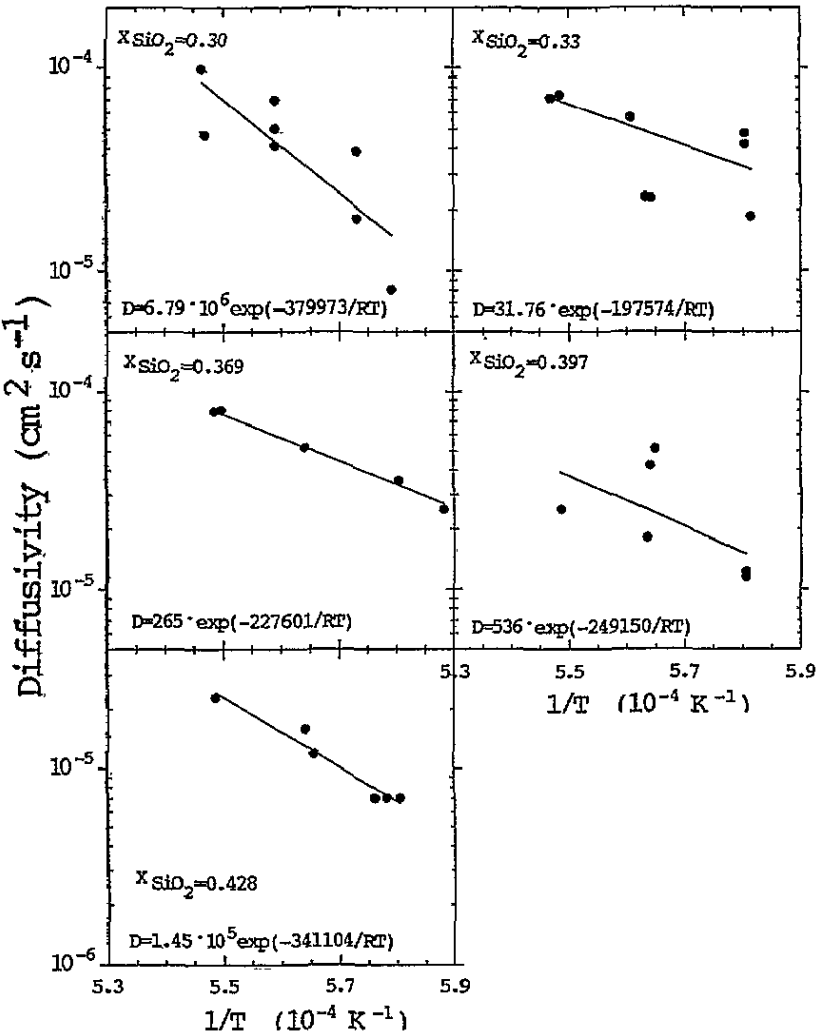

Figure 6. Arrhenius plots of oxygen tracer diffusivities for melts with various compositions.

2.2. *Analysis of diffusion profiles*

Before carrying out the actual isotope tracer diffusion experiment, we performed a preliminary experiment to check possible convection effects. A short-time chemical diffusion run in which a capillary contained a cobalt silicate melt with $X_{SiO_2} = 0.45$ and a reservoir melt with $X_{SiO_2} = 0.30$ was performed using the same boundary and initial conditions as described above. The results indicated that the convection effects were successfully suppressed. The chemical concentration (Si and Co) of the sample was analysed by an x-ray energy dispersive scanning electron microscope (SEM), and a smooth profile, without any effects of convection, was obtained. Figure 4 represents this profile.

Following this, the actual ^{18}O diffusion experiment was carried out. Figure 5 shows a typical concentration profile. For the given boundary and initial conditions, the analytical formula describing the resulting isotope concentration profile in a capillary with finite length is [18]:

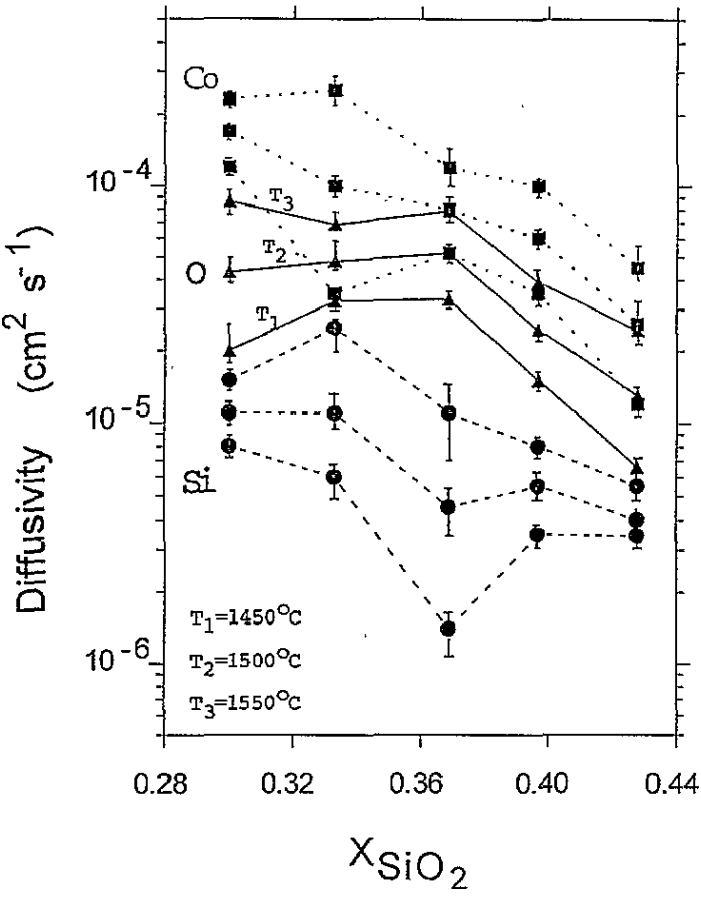

Figure 7. ^{18}O diffusivities as a function of composition: (■) ^{57}Co [14]; (●) ^{29}Si [14]; (▲) ^{18}O on CoO* (this work).

$$c_x - c_1 = (c_0 - c_1)\frac{4}{\pi}\sum_{n=1}^{\infty}\frac{1}{2n+1}\sin\left(\frac{(2n+1)\pi x}{2L}\right)\exp\left[-\left(\frac{(2n+1)\pi}{2L}\right)^2 Dt\right] \qquad (3)$$

where L is the length of the sample, c_0 and c_1 are constant concentration of ^{18}O in the sample (at $t \leqslant 0$) and in the melt reservoir (at $t \geqslant 0$) respectively, c_x is the concentration at the position x, and D is diffusivity. If the diffusion time t is not too long (for $L > 2(Dt)^{1/2}$), the solution for a semi-infinite half-space, which involves only a single error function, provides an adequate description as well.

3. Results and discussion

By fitting equation (3) to the experimental data, effective diffusivities $D_{^{18}O}$ were calculated, assuming that $D_{^{18}O}$ is constant with respect to time and location in the sample. In figure 6 these diffusivities are plotted as a function of the reciprocal temperature, for different

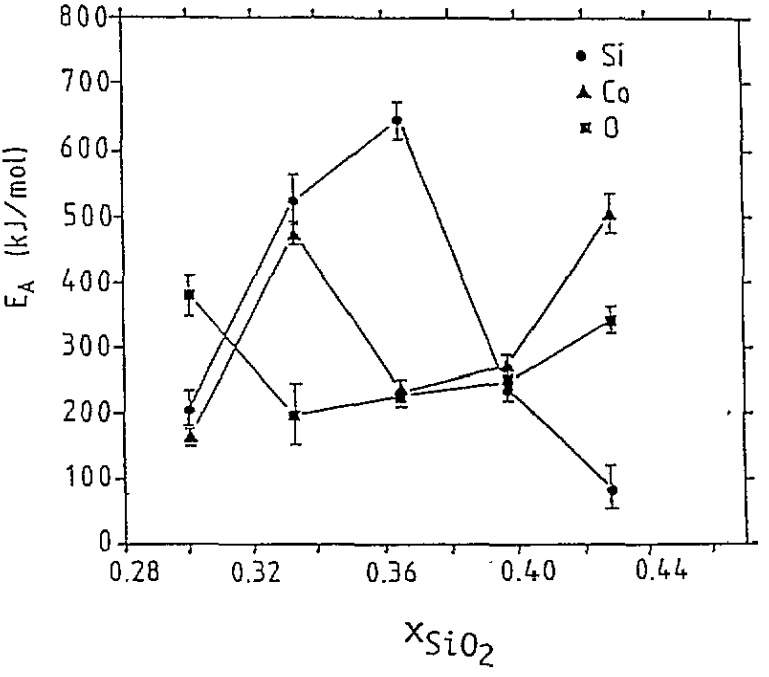

Figure 8. Activation energy of Co, Si and O diffusion as a function of composition (X_{SiO_2}).

compositions. The full line in each of these graphs represents the best fit of the Arrhenius relation

$$D = D_0 \exp(-E_A/RT)$$

to the data points. Here D_0 is the pre-exponential factor, R is the Boltzmann constant and E_A is the activation energy of oxygen diffusion. Figure 7 shows the tracer diffusivities of ^{18}O as a function of composition for three selected temperatures. For comparison, in the same figure, plots of the tracer diffusivities of cobalt and silicon are also shown. The magnitude of D decreases with increasing X_{SiO_2} which is the same behaviour as for Si and Co. It is clearly caused by variations in the polyanionic structure of the silicate melts.

Figure 8 shows the activation energies E_A for diffusion of O, Co and Si, plotted as a function of the composition. By comparing the results of Si, Co and O tracer diffusion, it was found that the composition dependence of the activation energy for oxygen diffusion was significantly smaller than those for silicon or cobalt diffusion. Also, at higher silica concentrations, the composition dependence of E_A for silicon exhibits a trend nearly opposite to that for oxygen or cobalt: above $X_{SiO_2} \simeq 0.369$ the activation energies for oxygen and cobalt diffusion increase steadily, whereas that for silicon decreases. Furthermore, at $X_{SiO_2} \simeq 0.33$ the activation energy for oxygen diffusion shows a minimum, while that for cobalt shows a maximum at the same composition. Silicon diffusivities are characterized by a maximum activation energy at $X_{SiO_2} = 0.369$. Further investigations are necessary for a better understanding of this behaviour.

When assuming the same mobility for all oxygen and silicon atoms present in the systems, the experimental diffusion profiles yield effective diffusion coefficients. On the other hand, the aforementioned kinetic model for silicate melts takes the difference in

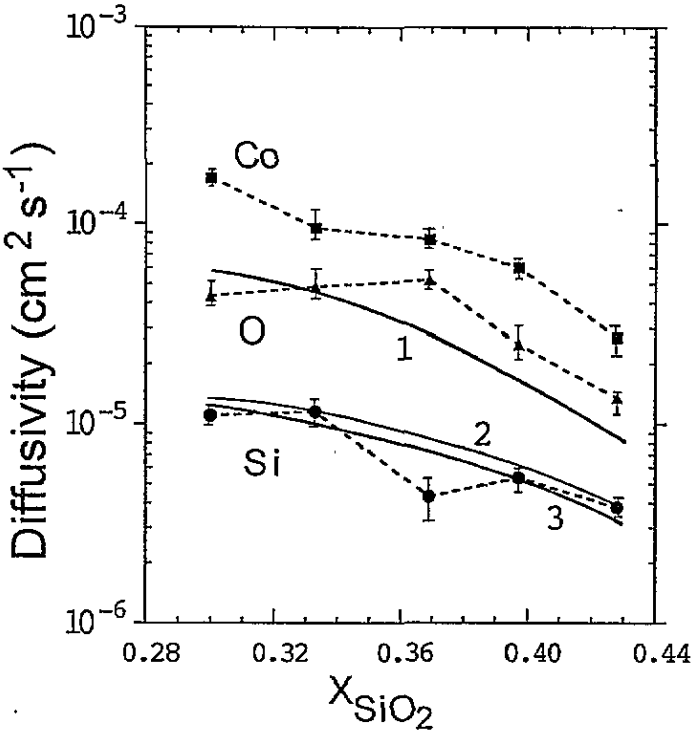

Figure 9. Tracer diffusivities in CoO–SiO_2 melts at $T = 1500\,°C$: (■) ^{57}Co [14]; (●) ^{29}Si [14]; (▲) ^{18}O on CoO*. Curves from simulations: 1, $Co^{18}O$; 2, $Si^{18}O_2$; 3, $^{29}SiO_2$.

mobilities of polyanions of various sizes, as well as condensation and splitting reactions between polyanions, into account. As a result, oxygen and silicon atoms move at different rates during different periods of time, depending on the size of the anion they belong to at that moment. Using this model we have simulated the oxygen tracer diffusion [17], and compared the resulting concentration profiles to the experimental ones. A satisfactory agreement between experimental and simulated profiles can only be obtained when assuming a strong tendency towards condensation in cobalt silicates. Under the same assumptions, the composition dependence of $D^*_{O,eff}$ is in good qualitative agreement with the experimental results, as shown in figure 9.

The comparison between samples containing $Co^{18}O$ and those containing $Si^{18}O_2$ as the tracer carriers show that ^{18}O diffusivities are lower in the latter case. In this case they are also rather close to the silicon diffusivities as measured by Kieffer [16]. The same behaviour is reported for the system CaO–SiO_2 [12, 19, 20].

4. Summary and conclusion

Oxygen tracer diffusion in the CoO–SiO_2 silicate melts was investigated by a capillary–reservoir method. A refined capillary design was employed for a convectionless diffusion experiment. Short-time diffusion experiments showed that convection was successfully suppressed. ^{18}O diffusion profiles were measured by SIMS analysis, using a modified sample preparation [15]. Best fits of the experimental data with analytical solutions of Fick's second

law for the appropriate initial and boundary conditions are consistently afflicted with subtle but systematic deviations. The diffusivities, $D^*_{O,eff}$, determined by such fits can therefore be considered as a measure of the effective transport rate, but they are not representative of the atomistic mechanisms involved in elemental diffusion.

The systematic deviations of experimental concentration profiles from ideal solutions and the composition dependence of $D^*_{O,eff}$ can be explained as due to the concurrent migration of differently sized species carrying tracer isotopes, and exchange reactions between these species [15, 16]. However, the composition dependence of the activation energies for oxygen, silicon and cobalt, which exhibit opposite trends, cannot be explained using the kinetic model for silicate melts. Further theoretical and experimental investigations are necessary for a better understanding.

Acknowledgments

We are indebted to E Ebeling for his experimental assistance. We also owe our thanks to the Deutsche Forschungsgemeinschaft for financial support. T F Young gratefully accepted a research fellowship from Technische Universität Clausthal.

References

[1] Toop G W and Samis C S 1963 *Can. Met. Q.* **1** 129
[2] Lin P L and Pelton A D 1979 *Metall. Trans.* B **10** 667
[3] Gaskell D R 1981 *Can. Met. Q.* **20** 3
[4] Masson C R 1965 *Proc. R. Soc.* A **287** 201
[5] Kapoor M L, Mehrotra G M and Frohberg M G 1974 *Arch. Eisenhüttenwes.* **45** 213
[6] Pretnar B 1968 *Ber. Bunsenges.* **72** 773
[7] Schmalzried H, Takada Y and Langanke B 1981 *Z. Phys. Chem.* **128** 205
[8] Petuskey W and Schmalzried H 1980 *Phys. Chem.* **84** 218
[9] Langanke B and Schmalzried H 1979 *Ber. Bunsenges. Phys. Chem.* **83** 59
[10] Keller H, Schwerdtfeger K and Hennesen K 1979 *Metall. Trans.* B **10** 67
[11] Keller H and Schwerdtfeger K 1979 *Metall. Trans.* B **10** 551
[12] Keller H, Schwerdtfeger K, Petri H, Hölze R and Hennesen K 1982 *Metall. Trans.* B **13** 237
[13] Frischat G H 1975 *Ionic Diffusion in Oxide Glasses* (Aedermannsdorf: Trans Tech)
[14] Kieffer J, Borchardt G, Scherrer S and Weber S 1986 *Mater. Sci. Forum* **7** 243
[15] Kieffer J and Borchardt G 1987 *Chem. Geol.* **62** 93
[16] Kieffer J and Borchardt G 1989 *Glastech. Ber.* **62** 337
[17] Young T F, Kieffer J and Borchardt G 1995 *J. Phys.: Condens. Matter* **6** 9835–52
[18] Tuck B 1974 *Introduction to Diffusion in Semiconductors (IEEE Monogr. Ser. 16)* (Stevenage: Peter Peregrinus) p 34
[19] Saito T, Shiraishi Y, Nishiyama N, Sorimachi K and Sawada Y 1973 *Fourth Japan–USSR Joint Symp. on Physical Chemistry of Metallurgical Processes* Iron and Steel Institute of Japan, p 53
[20] Shiraishi Y, Nagahama H and Ohta H 1983 *Can. Met. Q.* **22** 37